Effects of alloying element on stabilities, electronic structures, and mechanical properties of Pd–based superalloys*

Pei Yan(闫佩)[1], Xiao-Yu Chong(种晓宇)[2], Ye-Hua Jiang(蒋业华)[1], and Jing Feng(冯晶)[1,†]

[1] Faculty of Materials Science and Engineering, Kunming University of Science and Technology, Kunming 650093, China
[2] Department of Materials Science and Engineering, Pennsylvania State University, University Park, PA 16802, USA

(Received 28 July 2017; revised manuscript received 30 August 2017; published online 20 October 2017)

The thermodynamic stabilities, electronic structures, and mechanical properties of the Pd-based superalloys are studied by first principles calculations. In this work, we discuss the effect of Pd-based superalloys made from Al, Si, Sc, Ti, V, Cr, Mn, Fe, Cu, Zn, Y, Zr, Nb, Mo, Tc, Hf, Ta, W, Re, Os, Ir and Pt, and we also calculate a face centered cubic (fcc) structure $2\times2\times2$ superalloy including 31 Pd atoms and one alloying element TM ($Pd_{31}TM$). The mixing energies of these Pd-Based superalloys are negative, indicating that all Pd-based superalloys are thermodynamically stable. The $Pd_{31}Mn$ has the lowest mixing energy with a value of -0.97 eV/atom. The electronic structures of the Pd-based superalloys are also studied, the densities of states, elastic constants and moduli of the mechanical properties of the Pd-based superalloys are determined by the stress-strain method and Voigt–Reuss–Hill approximation. It is found that $Pd_{31}TM$ is mechanically stable, and $Pd_{31}Tc$ has the largest C_{11}, with a value 279.7 GPa. The $Pd_{31}Cr$ has the highest bulk modulus with a value of 299.8 GPa. The $Pd_{31}Fe$ has the largest shear modulus and Young's modulus with the values of 73.8 GPa and 195.2 GPa, respectively. By using the anisotropic index, the anisotropic mechanical properties of the $Pd_{31}TM$ are discussed, and three-dimensional (3D) surface contours and the planar projections on (001) and (110) planes are also investigated by the Young modulus.

Keywords: high temperature superalloy first-principles calculations, palladium mechanical properties, anisotropy

PACS: 62.20.de, 81.05.Xj, 71.20.–b, 71.23.–k **DOI:** 10.1088/1674-1056/26/12/126202

1. Introduction

Due to the fact that platinum-group-metals (PGMs) have excellent physical and mechanical properties, they have received a great deal of attention from high-temperature applications.[1–7] The PGMs have the same face centered cubic (fcc) structures as Ni-Based superalloys.[8] Pan has studied the structure, electronic and elastic properties of $RuAl_2$ of typical $TiSi_2$-type structure.[9] Among the platinum-group-metals, the melting-point of Palladium is 1837 K, which is higher than those of Ni-based superalloys. With one or more alloy element added, the mechanical properties of Pd-based superalloys have been obviously improved.[10,11] Ning *et al.*'s study showed that the rare earth elements not only improve the room temperature strength and elasticity of Pd, but also increases the high temperature instantaneous strength, creep life and activation energy of Pd.[12] Zhou has studied the microstructure and mechanical properties of Pd–Ag–Cu alloy.[13] Wang *et al.* showed that the addition of Rh significantly improves the mechanical properties of Pd–Rh–V.[10] To investigate the development of the Pd-based superalloys, it is desirable to gain the effects of alloying elements on Pd-based superalloys. In this work, we investigate the thermodynamic stability, electronic structures, and mechanical properties of the Pd-based superalloys. To understand the thermodynamic stability of the Pd-based superalloys, we calculate the mixing of their energies. We also calculate the total density of states, the partial density of states via first principles calculation, to study the electronic structures of the Pd-based superalloys. The modulus of elasticity measures the ability of the material to recover shape after deformation and provide information of the deformation behavior of the material. The single crystals are anisotropic. The occurrence of micro cracks in materials is always related to anisotropy; therefore, it is necessary to describe the parameter of the anisotropy. In this work, the following 21 alloying elements in Pd-based superalloys are determined: Al, Si, Sc, Ti, V, Cr, Mn, Fe, Cu, Zn, Y, Zr, Nb, Mo, Tc, Hf, Ta, W, Re, Os, Ir, and Pt. We calculate the structural stability, electronic structure and mechanical properties of $Pd_{31}TM$ via first principles calculations.

2. Computational method and details

In this work, we calculate a face centered cubic (fcc) structure $2\times2\times2$ superalloy including 31 Pd atoms and one alloying element TM. The first principles calculation is based on density functional theory (DFT), using the Cambridge Serial Total Energy Package (CASTEP) code.[14,15]

*Project supported by the Young-Talent Support Programs of Kunming University of Science and Technology, China (Grant No. 11504146) and the National Natural Science Foundation of China (Grant No. 51762028).

†Corresponding author. E-mail: jingfeng@kmust.edu.cn

© 2017 Chinese Physical Society and IOP Publishing Ltd

The relation between valence electrons and ionic solid was described by the generalized gradient approximation (GGA) of the Perdew–Burke–Ernzerhof for surfaces for solids (PBEsol) approach.[16] The plane wave cutoff energy was 500 eV. In the first irreducible Brillouin zone, the k-point method used the ultrasoft pseudopotential. The exchange correlation energy was described by the GGA combined with the Monkhorsr-Pack method,[17] and a Monkhorst-Pack k-point mesh was $1\times1\times1$ of the $Pd_{31}TM$. In the geometric optimization process, the total energy change ultimately converges to 2×10^{-6} eV per atom and the force acting on an atom decreased to 0.01 eV/Å per atom. The valence electron configurations investigated in this work are chosen as follows: Pd $4d^2$, Al $3s^23p^1$, Si $3s^23p^2$, Sc $3d^14s^2$, Ti $3d^24s^2$, V $3d^34s^2$, Cr $3d^54s^1$, Mn $3d^54s^2$, Fe $3d^64s^2$, Cu $3d^{10}4s^1$, Zn $3d^{10}4s^2$, Y $4d^15s^2$, Zr $4d^25s^2$, Nb $4d^45s^1$, Mo $4d^55s^1$, Tc $4d^55s^2$, Hf $4f^{14}5d^26s^2$, Ta $4f^{14}5d^36s^2$, W $4f^{14}5d^46s^2$, Re $4f^{14}5d^56s^2$, Os $4f^{14}5d^66s^2$, Ir $4f^{14}5d^76s^2$, and Pt $4f^{14}5d^96s^1$.

3. Results and discussion

3.1. Structure characteristics and stability

In this paper, the dilute solution of the $Pd_{31}TM$ is shown in Fig. 1. The thermodynamic stability of the $Pd_{31}TM$ superalloy is determined by the mixing energy.

The energy parameters can be defined by the following expressions:

$$\Delta H_r\left(\mathrm{Pd}_x TM_y\right)=\frac{E_{\mathrm{tot}}\left(\mathrm{Pd}_x TM_y\right)-xE_{\mathrm{bin}}\left(Pd\right)-yE_{\mathrm{bin}}\left(TM\right)}{x+y}, \quad (1)$$

where $\Delta H_r\left(\mathrm{Pd}_x TM_y\right)$ is the mixing energy of $Pd_{31}TM$, $E_{\mathrm{tot}}\left(\mathrm{Pd}_x TM_y\right)$ is the total energy of $Pd_{31}TM$, $E_{\mathrm{bin}}\left(Pd\right)$ and $E_{\mathrm{bin}}\left(TM\right)$ are the crystals of Pd and TM, respectively.

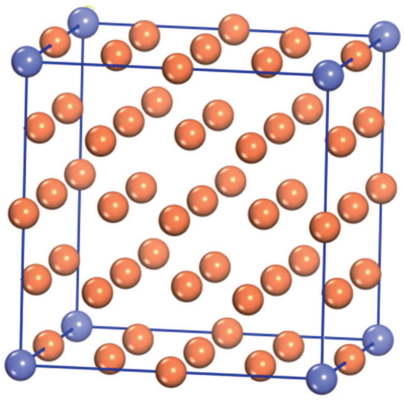


Fig. 1. (color online) Dilute solutions of $Pd_{31}TM$ (TM = Al, Si, Sc, Ti, V, Cr, Mn, Fe, Cu, Zn, Y, Zr, Nb, Mo, Tc, Hf, Ta, W, Re, Os, Ir, Pt).

For the dilute solution of thermodynamic stability, the mixing energy of $Pd_{31}TM$ is negative, and the lower the negative value, the more stable the dilute solution is. In this work, the density, volume, and mixing energy of the $Pd_{31}TM$ superalloy are listed Table 1. In Table 1, the values of the mixing energy of all $Pd_{31}TM$ are negative, indicating that they are thermodynamically stable. From Table 1, we can see the value of the mixing energy of $Pd_{31}Mn$ is smallest with a value of -0.97 eV/atom, suggesting that $Pd_{31}Mn$ is most stable. The $Pd_{31}Pt$ has the highest mixing energy, indicating that $Pd_{31}Pt$ is less stable than the other $Pd_{31}TM$. The values of the mixing energy of $Pd_{31}Pt$ are -0.03 eV/atom and -4.74 eV/atom, respectively.

Table 1. Values of denisty, volume, mixing energy (ΔH_r) of $Pd_{31}TM$ superalloys.

Species	ρ/gcm^{-3}	V/Å^3	ΔH_r/(eV/atom)
$Pd_{31}Al$	11.86	465.5	–0.10
$Pd_{31}Si$	11.90	463.7	–0.86
$Pd_{31}Sc$	11.83	469.1	–0.04
$Pd_{31}Ti$	11.91	466.5	–0.11
$Pd_{31}V$	11.97	463.7	–0.32
$Pd_{31}Cr$	12.00	463.7	–0.41
$Pd_{31}Mn$	11.56	480.0	–0.97
$Pd_{31}Fe$	11.50	480.0	–0.73
$Pd_{31}Ni$	12.01	463.7	–0.15
$Pd_{31}Cu$	12.02	463.7	–0.08
$Pd_{31}Zn$	12.01	465.5	–0.01
$Pd_{31}Y$	11.85	474.6	–0.05
$Pd_{31}Zr$	11.95	471.1	–0.13
$Pd_{31}Nb$	11.87	474.6	–0.08
$Pd_{31}Mo$	12.08	467.3	–0.06
$Pd_{31}Tc$	12.12	465.5	–0.58
$Pd_{31}Hf$	12.22	472.6	–0.11
$Pd_{31}Ta$	12.27	472.6	–0.15
$Pd_{31}W$	12.39	466.5	–0.06
$Pd_{31}Re$	12.42	465.5	–0.42
$Pd_{31}Os$	12.44	465.5	–0.57
$Pd_{31}Pt$	12.40	466.5	–0.03

The change of the mixing energy of $Pd_{31}TM$ with the atomic radius increases is shown in Fig. 2. From Fig. 2, we clearly see that $Pd_{31}Mn$ is the most stable system, and 4d transition metal alloying elements are relatively unstable compared with other 3d, 5d transition metal alloying elements.

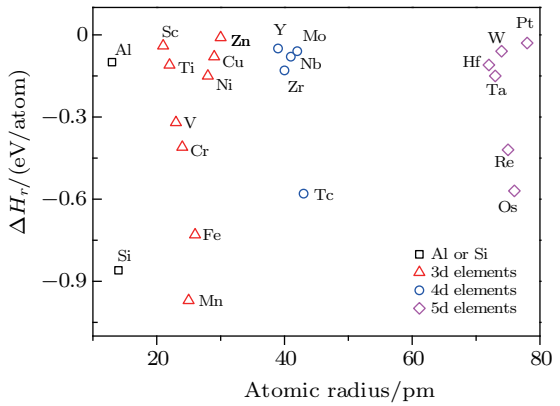


Fig. 2. (color online) Variations of mixing energy with atomic radius of $Pd_{31}TM$.

3.2. Electronic structure

In this paper, in order to study the chemical bond properties and electronic structures of $Pd_{31}TM$, the total density of state (TDOS), partial density of state (PDOS), electron density distribution and the electron density difference map of $Pd_{31}TM$ superalloys are calculated.

Figure 3 shows the calculated total densities of state (TDOSs) and partial densities of state (PDOSs) of the $Pd_{31}TM$. It is shown from the diagram that none of all the $Pd_{31}TM$ has the band gap at the Fermi level, indicating that $Pd_{31}TM$ are strongly metallic and they are electrically conductive. The trend of the total electron density at the Fermi level is the same as that of the Pd-4d orbital, indicating that the density of the electron states at the Fermi level is dominated by the Pd-4d orbital, the band ranges from −5 eV to 1 eV. The orbital of Pd-4d is different from those of transition metals (TM), indicating that all $Pd_{31}TM$ superalloys have strong metal bonds. For $Pd_{31}Al$ and $Pd_{31}Si$, the densities of states at the Fermi level are very similar. For 3d elements, the total density of states is the same as that for Pd-4d at the Fermi level. In all of the 3d elements of $Pd_{31}TM$, except for $Pd_{31}Fe$, the maximal density of states of Pd-4d of other 3d elements is about 2 eV, and the maximal density of states of $Pd_{31}Fe$ is 1 eV. For 4d elements of $Pd_{31}TM$, the change of the total density of states and Pd-4dhave the same trend. In addition to $Pd_{31}Zr$, for 5d elements, the total density of states is similar to the trend of Pd-4d, and the density of states on the Pd-4d orbit has a maximal value, which is about 1.8 eV.

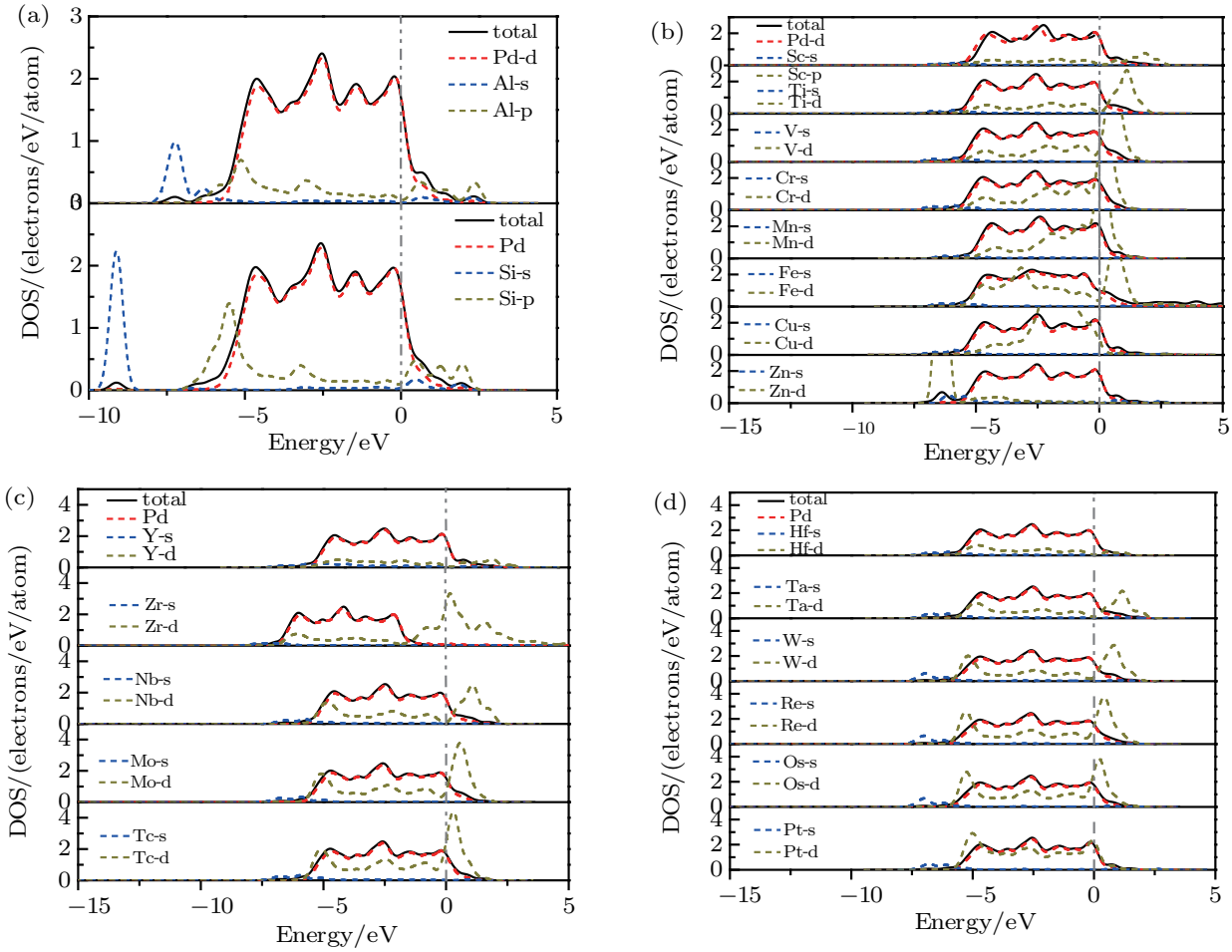


Fig. 3. (color online) Calculated total densities of states and partial densities of states for $Pd_{31}TM$. Dash line represents the Fermi level. Panels (a), (b), (c) and (d) show the densities of states and partial densities of states of Al, Si, 3d, 4d and 5d elements, respectively.

3.3. Elastic properties and moduli

In this paper, the elastic constants of $Pd_{31}TM$ are obtained by the stress-strain method based on the generalized Hooke law, then all elastic modulus (C_{ij}), bulk modulus (B), shear modulus (G) and Young modulus (E) of $Pd_{31}TM$ superalloys are obtained by the Voigt–Ruess–Hill method,[18] C_{11}, C_{22} and C_{33} are the compressive resistances of crystal along the [001], [010], and [100] crystallographic directions, and C_{44}, C_{55}, and C_{66} represent the ability to shear strain on the crystal faces (001), (010), and (100). For a cubic system, C_{11} is the largest in all independent elastic constants. The calculated elastic constants of all $Pd_{31}TM$ are C_{11}, C_{12}, and C_{44}, respectively. In order to study the mechanical stability of the $Pd_{31}TM$ system,

the stability of the $Pd_{31}TM$ system is further investigated. The formula for the mechanical stability is discussed by the elastic constants of the dilute solution; the formula for the mechanical stability of cubic systems is as follows:[19]

$$(C_{11}-C_{12})>0_{11}>0,\quad C_{44}>0,$$
$$C_{11}+2C_{12}>0. \tag{2}$$

Table 2. Calculated values of elastic constant (C_{ij}) in units of GPa, bulk modulus (B), shear modulus (G), Young's modulus (E), which are in units of GPa, B/G, and Poisson's ratio of $Pd_{31}TM$.

Species	C_{11}	C_{12}	C_{44}	B	G	E	B/G	σ
[a]Pd	234.1	176.1	71.2	195.5	44.9	125.1	4.4	0.39
Pd[cal]	254.0	197.1	86.1	216.1	55.29	152.8	3.9	0.38
$Pd_{31}Al$	243.0	201.8	89.9	216.1	50.6	140.8	4.27	0.39
$Pd_{31}Si$	250.2	202.7	90.7	218.7	53.2	147.6	4.11	0.38
$Pd_{31}Sc$	250.1	194.5	94.3	212.6	58.4	160.6	3.64	0.37
$Pd_{31}Ti$	249.9	193.1	108.7	188.2	70.5	188.0	2.67	0.33
$Pd_{31}V$	267.9	172.8	100.0	185.3	62.6	168.8	2.96	0.35
$Pd_{31}Cr$	259.8	207.1	100.79	299.8	63.4	177.7	4.73	0.40
$Pd_{31}Mn$	217.7	206.9	79.5	200.4	47.4	131.7	4.23	0.39
$Pd_{31}Fe$	254.9	147.9	91.5	183.5	73.8	195.2	2.48	0.32
$Pd_{31}Cu$	241.8	203.1	90.4	216.0	51.3	142.5	4.21	0.39
$Pd_{31}Zn$	246.6	197.4	89.8	213.0	54.2	149.9	3.93	0.38
$Pd_{31}Y$	254.4	202.2	94.6	219.1	56.4	155.9	3.88	0.36
$Pd_{31}Zr$	267.1	189.6	96.5	215.2	66.6	181.1	3.23	0.36
$Pd_{31}Nb$	245.7	183.8	94.9	204.4	60.6	165.4	3.37	0.37
$Pd_{31}Mo$	272.5	203.6	104.9	225.1	66.7	182.2	3.37	0.37
$Pd_{31}Tc$	279.4	206.9	103.6	227.3	67.1	183.2	3.39	0.37
$Pd_{31}Hf$	267.1	191.6	96.9	217.1	66.6	181.3	3.26	0.36
$Pd_{31}Ta$	266.1	201.3	101.8	221.4	63.6	174.3	3.48	0.37
$Pd_{31}W$	265.8	198.0	105.8	223.1	67.8	184.6	3.29	0.30
$Pd_{31}Re$	272.4	199.5	107.1	222.1	69.2	188.0	3.21	0.36
$Pd_{31}Os$	269.6	202.3	101.8	23.1	66.5	181.4	3.35	0.36
$Pd_{31}Pt$	240.7	210.9	85.0	220.9	43.2	121.6	5.11	0.41

[a]Cal. in Ref. [21].

In Table 2, we can see that the elastic constants of $Pd_{31}TM$ satisfy the above formulas, indicating that the $Pd_{31}TM$ superalloy is mechanically stable. These elastic constants (C_{ij}) of $Pd_{31}TM$ superalloy are obtained, bulk modulus (B), shear modulus (G), Young modulus (E) and Poisson ratio (σ) are obtained by the Voigt–Ruess–Hill approximation method, and the formulas are as follows:[20–24]

$$B_{\mathrm{VRH}}=B_{\mathrm{R}}=B_{\mathrm{V}}=\frac{1}{3}(C_{11}+2C_{12}), \tag{3}$$

$$G_{\mathrm{V}}=\frac{1}{5}(C_{11}-C_{12}+3C_{44}), \tag{4}$$

$$G_{\mathrm{R}}=\frac{5(C_{11}-C_{12})C_{44}}{4C_{44}+3(C_{11}-C_{12})}, \tag{5}$$

$$G_{\mathrm{VRH}}=\frac{1}{2}(G_{\mathrm{V}}+G_{\mathrm{R}}), \tag{6}$$

$$E=\frac{9B_{\mathrm{VRH}}G_{\mathrm{VRH}}}{3B_{\mathrm{VRH}}+G_{\mathrm{VRH}}}, \tag{7}$$

$$\sigma=\frac{3B_{\mathrm{VRH}}-2G_{\mathrm{VRH}}}{2(3B_{\mathrm{VRH}}+G_{\mathrm{VRH}})}, \tag{8}$$

where B_{VRH}, B_{R}, and B_{V} are the bulk moduli calculated by Voigt–Reuss–Hill, Reuss and Voigt approximation methods, respectively. G_{VRH}, G_{R}, and G_{V} are the shear moduli calculated by Voigt–Reuss–Hill, Reuss, and Voigt approximation methods, respectively.

The results of elastic constants and moduli of Pd-Based superalloy from calculations and experiments of Pd are listed in Table 2. It is found that the trends of 3d, 4d, and 5d transition metal alloying elements toward the mechanical properties for $Pd_{31}TM$ are increasing. The $Pd_{31}Tc$ has the largest C_{11}, indicating that $Pd_{31}Tc$ has the highest compressive resistance under uniaxial stress along the crystallographic x axis direction. The value of C_{11} of $Pd_{31}Tc$ is 279.38 GPa. The $Pd_{31}Re$ has the largest C_{44} (107.1 GPa), suggesting that $Pd_{31}Re$ has the strongest ability to shear strain on the (001) crystal face. In the $Pd_{31}TM$ superalloy, $Pd_{31}Cr$ has the largest bulk modulus, indicating that $Pd_{31}Cr$ has the most compression resistance under hydrostatic pressure. The shear modulus reflects the deformation resistance under shear stress, and the Young modulus reflects a ruler of the stiffness of materials. The $Pd_{31}Fe$ has the largest shear modulus and Young modulus, 73.79 GPa and 195.21 GPa, respectively, which indicates that the $Pd_{31}Fe$ has the strongest deformations resistance under shear stress and the largest stiffness. The value of B/G usually indicates the brittleness or ductility of a compound.[20] When the value of the B/G ratio is greater than 1.75, the material presents the ductile characteristics.[21] From Table 2, all of $Pd_{31}TM$ superalloys are ductile. Poisson's ratio represents the elastic constant of material transverse deformation, and the Poisson ratio is close to 0.3; the materials have the metallic bonding features. The Poisson ratio of $Pd_{31}W$ is 0.30, suggesting that it has a metallic bond and is easy to form.

In order to further understand the effects of the elements on the elasticity of $Pd_{31}TM$ superalloy, the elastic moduli varying with the density of $Pd_{31}TM$ are plotted in Fig. 4. It is clearly found that the 3d, 4d, and 5d alloying elements lead to the bulk modulus of $Pd_{31}TM$ increasing linearly. Within each group of 4d and 5d elements, the bulk modulus of $Pd_{31}TM$ increases with the density of $Pd_{31}TM$ increasing. Of shear moduli, the modulus of 5d elements of $Pd_{31}TM$ are the largest. For Poisson's ratio and B/G, we can see that they have the same change trends.

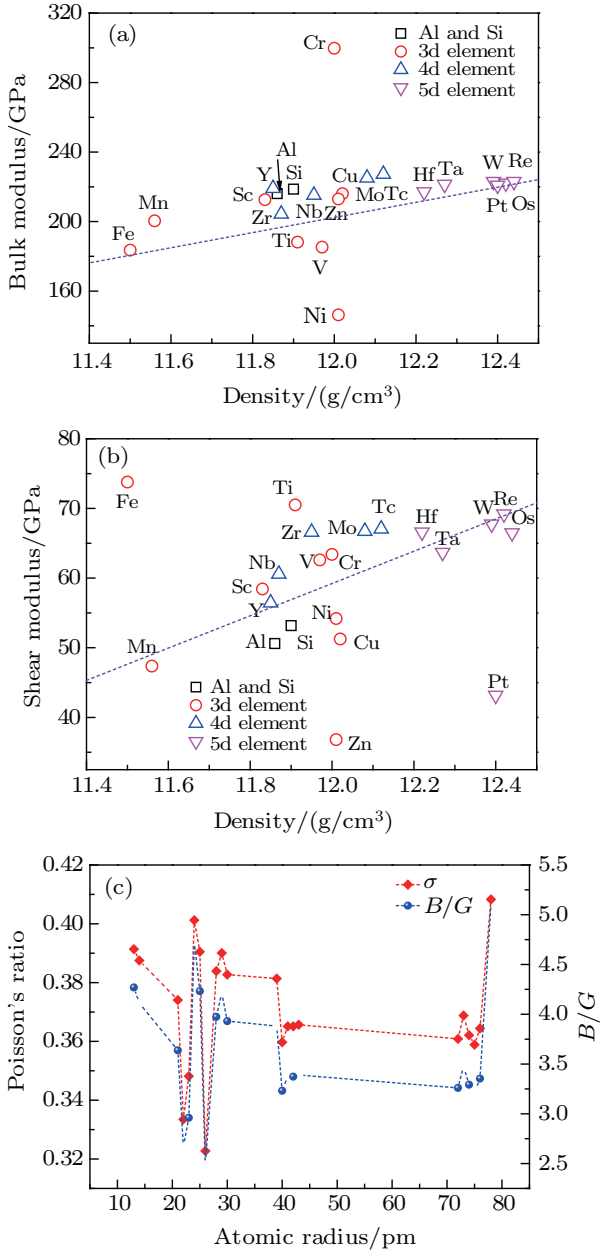


Fig. 4. (color online) Variations of (a) the bulk modulus of $Pd_{31}TM$, (b) the shear modulus of $Pd_{31}TM$, and (c) Poisson's ratio and B/G of $Pd_{31}TM$.

3.4. Mechanical anisotropy

In this work, we calculate the mechanical anisotropy of $Pd_{31}TM$. The anisotropy is related to the micro cracks in a material; therefore, it is necessary to describe the anisotropy of $Pd_{31}TM$. In order to understand anisotropy, we calculate the universal anisotropic index (A^{U}) and percent of anisotropic index (A^{B} and A^{G}), as follows:[24,25]

$$A^{U} = 5\frac{G_V}{G_R} + \frac{B_V}{B_R} - 6 \geq 0, \tag{9}$$

$$A_B = \frac{B_V - B_R}{B_V + B_R}, \tag{10}$$

$$A_G = \frac{G_V - G_R}{G_V + G_R}, \tag{11}$$

where B_V, B_R, G_V, and G_R are the bulk modulus and shear modulus estimation within Voigt and Reuss approximations, respectively. The results of anisotropic index are listed in Table 3. The value of the anisotropy index is close to zero, so the material is anisotropic. The universal anisotropic index A^{U} is the indicator to reflect the anisotropy of the elastic property. The $Pd_{31}Pt$ has the largest A^{U} and A_G, indicating that the elasticity and the shear of $Pd_{31}Pt$ are mostly anisotropic.

Table 3. Calculated values of universal anisotropic index (A^{U}), anisotropy (A_B and A_G) of $Pd_{31}TM$.

Species	A^{U}	A_B	A_G
$Pd_{31}Al$	2.9	0	0.2
$Pd_{31}Si$	2.5	0	0.2
$Pd_{31}Sc$	1.9	0	0.2
$Pd_{31}Ti$	1.4	0	0.1
$Pd_{31}V$	2.1	0.1	0.2
$Pd_{31}Cr$	1.9	0	0.2
$Pd_{31}Mn$	2.6	0.1	0
$Pd_{31}Fe$	0.4	0	0
$Pd_{31}Cu$	2.9	0	0.2
$Pd_{31}Zn$	2.3	0	0.2
$Pd_{31}Y$	2.3	2.3	0.2
$Pd_{31}Zr$	1.0	0	0.2
$Pd_{31}Nb$	1.7	0	0.1
$Pd_{31}Mo$	1.7	0	0.1
$Pd_{31}Tc$	1.6	0	0.1
$Pd_{31}Hf$	1.1	0	1.0
$Pd_{31}Ta$	1.8	0	0.2
$Pd_{31}W$	1.7	0	0.1
$Pd_{31}Re$	1.6	0	0.1
$Pd_{31}Os$	1.5	0	0.1
$Pd_{31}Pt$	4.7	0	0.3

To better understand the characteristic of elastic anisotropy, we plot the three-dimensional (3D) surface of $Pd_{31}TM$. The Young modulus is plotted in spherical coordinates. The 3D representation of Young's modulus for cubic crystal is given by the following equations:[26]

$$\frac{1}{E} = s_{11} - 2\left(s_{11} - s_{12} - \frac{1}{2}s_{44}\right)\left(l_1^2 l_2^2 + l_2^2 l_3^2 + l_3^2 l_1^2\right), \tag{12}$$

where s_{ij} is the elastic compliance matrix, l_1, l_2, and l_3 are the directional cosines. The adoption of the relationship of the direction cosines in spherical coordinates with respect to θ and ψ yields $l_1 = \sin\theta\cos\psi$, $l_2 = \sin\theta\sin\psi$, and $l_3 = \cos\psi$. The obtained surface contours of the Young modulus are illustrated in Fig. 5. We clearly see that the $Pd_{31}Pt$ has the strong anisotropy. The $Pd_{31}Fe$ has the weakest anisotropy in Young's modulus.

Figure 6 shows the anisotropic properties of the Young modulus of $Pd_{31}TM$ on the (001) and (110) planes. For 3d elements, the planar contour of $Pd_{31}Fe$ has a maximal Young

modulus along the axis. The $Pd_{31}Mn$ has a minimal Young modulus. For 4d elements, the planar contour of $Pd_{31}Zr$ has a maximal Young modulus along the axis. The $Pd_{31}Y$ has a minimal Young modulus. For 5d elements, the planar contour of $Pd_{31}Re$ has a maximal Young modulus along the axis. The $Pd_{31}Pt$ has a minimal Young modulus.

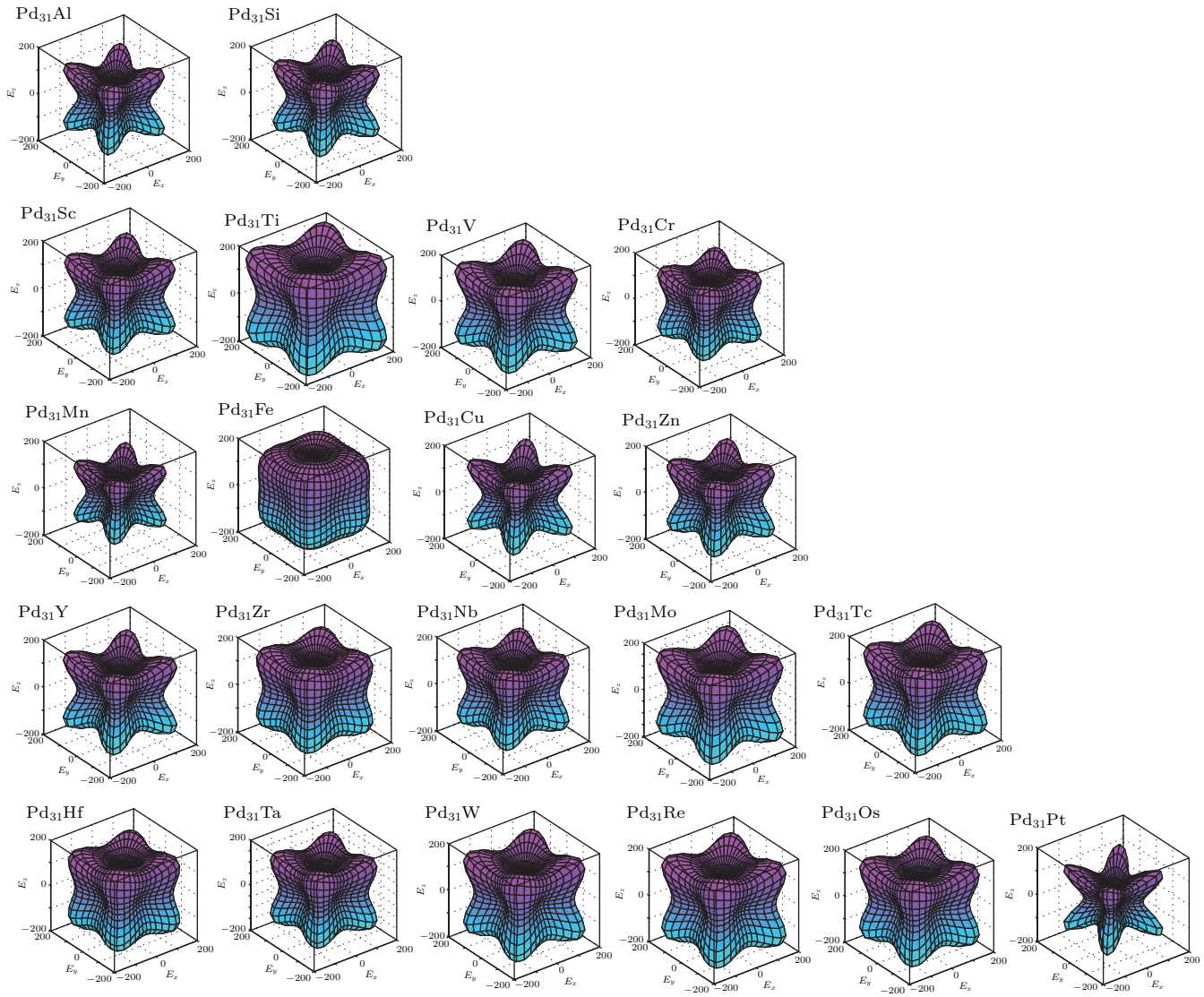


Fig. 5. (color online) Surface contours of the Young modulus of $Pd_{31}TM$.

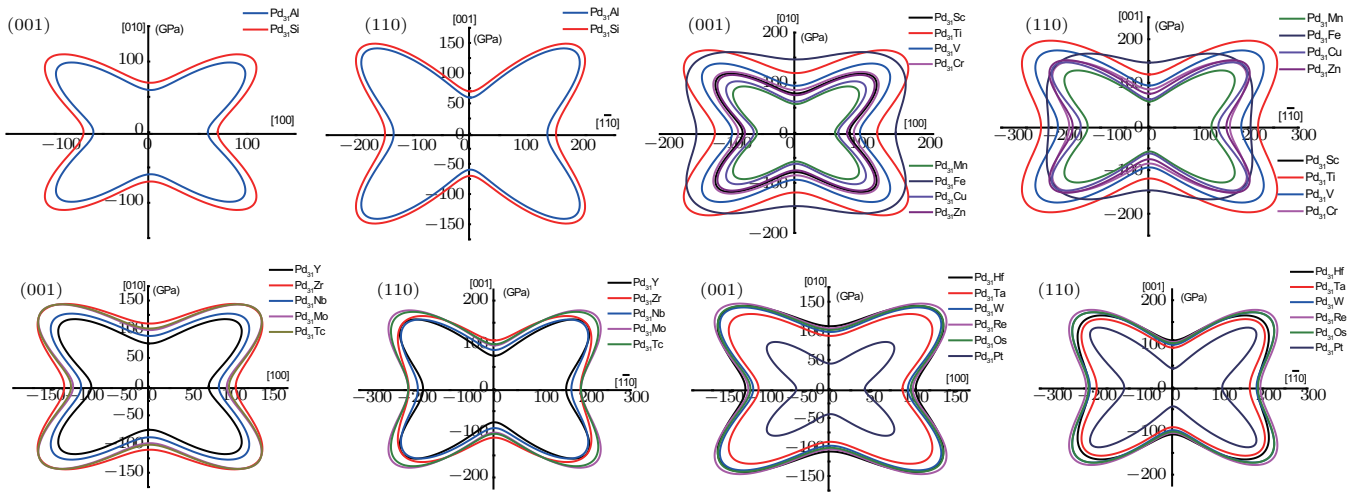


Fig. 6. (color online) Planar projections of the Young moduli of the $Pd_{31}TM$ on the (a) (001) and (b) (110) crystallographic planes.

4. Conclusions

The thermodynamic stabilities, electronic structures, and mechanical properties of the Pd-based superalloys are studied by first principles calculations. The mixing energies of these Pd-based superalloys are negative, so the $Pd_{31}TM$ (TM = Al, Si, Sc, Ti, V, Cr, Mn, Fe, Cu, Zn, Y, Zr, Nb, Mo, Tc, Hf, Ta, W, Re, Os, Ir, and Pt) are thermodynamically stable. The electronic structures of the Pd-based superalloys are also studied. The bonding characteristics of the $Pd_{31}TM$ superalloys are dominated by metallic bonds. The elastic constants and moduli of the mechanical properties of the Pd-based superalloys are determined by the stress-strain method and Voigt–Reuss–Hill approximation. It is found that $Pd_{31}TM$ are mechanically stable, and Pd_{31}Tc has the largest C_{11}, with a value of 279.7 GPa. The Pd_{31}Cr has the highest bulk modulus, with a value of 299.8 GPa. The Pd_{31}Fe has the largest shear modulus and Young's modulus, whose values are 73.8 GPa and 195.2 GPa, respectively. In this work, we summarize the systematical theoretical researches of $Pd_{31}TM$ superalloys, and the fundamental physical picture of the properties of the compound can be established, which will be useful for the experimental research and applications of Pd-based superalloys in the future.

References

[1] Alam M Z, Kamat S, V Jayaram V. and Das D K 2014 *Acta Mater.* **67** 278

[2] Alam M Z, Srivathsa B, Kamat S V, Jayaram V and Das D K 2011 *Mater. Des.* **32** 1242.

[3] Biesiekierski A, Ping D H, Mitarai Y Y and Wen C 2014 *Mater Des.* **59** 303

[4] Alam M Z, Kamat S V, Jayaram V, and Das D K 2013 *Acta Mater.* **61** 1093

[5] Grushko B, Kapush D, Su J and Wan W 2013 *J. Alloys Compd.* **580** 618

[6] Xing W W, Chen X Q, Li D Z, *et al.* 2012 *Intermetallics* **28** 16

[7] Pan Y and Lin Y 2016 *J. Alloys Compd.* **684** 171

[8] Rheaume J M, Mtiller B and Schulze M 1998 *J. Power Sources* **76** 60

[9] Pan Y 2017 *Mater. Res. Bull.* **93** 56

[10] Wang T F, Chen P, Deng Y H and Tang B Y 2011 *Trans. Nonferrous Met. Soc. China* **21** 388

[11] Yan P, Chong X Y, Jiang Y H and Feng J 2017 *J. Alloys Compd.* **710** 589

[12] Ning Y T, Wen F, Zhao Z H and Deng D G 1994 *Precious Metals* **15** 32 (in Chinese)

[13] Zhou S P 1999 *Rare Metals* **4** 20 (in Chinese)

[14] Segall M D, Lindan P J D, Probert M J, Probert C J, Hasnip P J, Clark J. and Payne M C 2002 *J. Phys: Condens Matter.* **14** 2717

[15] Hu M Y, Yu J, Zhou X L, Hong Z J and Ye W 2016 *Rare Metal* **4** 1

[16] Perdew J P, Ruzsinszky A, Csonka G I, *et al.* 2008 *Phys. Rev. Lett.* **100** 136406

[17] Monkhorst H J and Pack J D 1976 *Phys. Rev. B* **13** 5188

[18] Chung D H and Buessem W R 1967 *J. Appl. Phys.* **38** 2535

[19] Mouhat F and Coudert F X 2014 *Phys. Rev. B* **90** 224104

[20] Hill R, Proc 1952 . *Phys. Soc. A.* **65** 349

[21] Rayne J A 1960 *Phys. Rev.* **118** 1545

[22] Chong X Y, Jiang Y H and Feng J 2017 *J. Micromech. Mol. Phys.* **2** 1750002

[23] Liu Y H, Chong X Y, Jiang Y H and Feng J 2017 *Chin. Phys. B* **26** 037102

[24] Ranganathan S I and Ostoja-Starzewski M 2008 *Phys. Rev. Lett.* **101** 055504

[25] Liu Y H, Chong X Y, Jiang Y H, Zhou R and Feng J. 2017 *Phys. B* **506** 1

[26] Chong X Y,Jiang Y H, Zhou R, Zhu H and Feng J 2015 *Comput. Mater. Sci.* **108** 205